Natural Hazards
and Earth System
Sciences

Wildfire–atmosphere interaction index for extreme-fire behaviour

Tomàs Artés[1], **Marc Castellnou**[2], **Tracy Houston Durrant**[3], **and Jesús San-Miguel**[1]

[1]Joint Research Centre (JRC), European Commission, Ispra, Italy
[2]Grup de Recolzament a Actuacions Forestals (GRAF), Generalitat de Catalunya, Carretera de l'Autònoma,
s/n. 08290 Cerdanyola del Vallès, Spain
[3]Engineering Ingegneria Informatica S.p.A., European Commission, Rome, Italy

Correspondence: Tomàs Artés (tomas.artes-vivancos@ec.europa.eu)

Abstract. During the last 20 years extreme wildfires have challenged firefighting capabilities. Often, the prediction of the extreme behaviour is essential for the safety of citizens and firefighters. Currently, there are several fire danger indices routinely used by firefighting services, but they are not suited to forecast extreme-wildfire behaviour at the global scale. This article proposes a new fire danger index, the extreme-fire behaviour index (EFBI), based on the analysis of the vertical profiles of the atmosphere above wildfires as an addition to the use of traditional fire danger indices. The EFBI evaluates the ease of interaction between wildfires and the atmosphere that could lead to deep moist convection and erratic and extreme wildfires. Results of this research through the analysis of some of the critical fires in the last years show that the EFBI can potentially be used to provide valuable information to identify convection-driven fires and to enhance fire danger rating schemes worldwide.

1 Introduction

Fires have naturally occurred in nearly all world biomes, shaping ecosystems and landscapes, but are intrinsically linked to human activities. As humans spread to colonize most regions of the world, they brought fire with them and used it as a tool in agriculture and cattle-raising activities. Currently, over 90 % of the fires that occur in the world are caused by humans, deliberately or accidentally (Balch et al., 2017; Short, 2017; San-Miguel-Ayanz et al., 2012). In most regions of the world the most prominent fire management policy is that of fire exclusion. Fires that are purposely or accidentally started affect human assets and are thus controlled

and extinguished as fast as possible. Only fires in very high latitudes, where human dwellings do not exist, are left to burn naturally. In the context of this paper we use the term wildfires, referring to those fires that escape beyond human control and cause damage to human lives and property. Nowadays, it is estimated that about 400 million hectares of natural and agricultural lands are burnt annually, although it is recognized that this figure is likely a gross underestimate of the total area burnt in reality (Boschetti et al., 2019). Wildfires are responsible for vast economic and environmental damage, the loss of human lives, and about 17 % of the global CO_2 (Shi et al., 2015; Friedlingstein et al., 2019) emissions. Most wildfires occur in the vicinity of humans, as they are caused by humans, and thus they affect people and human assets in the area where they occur. In Europe, this intermingling of human dwellings and natural areas is referred to as the wildland–urban interface (WUI) and corresponds to the area where most fires and burnt areas occur.

The damage caused by fires in the WUI is thus much greater than that of fires occurring in remote areas due to the high adaptability of ecosystems in those areas (Pausas and Keeley, 2009, 2017). In recent years, the occurrence of extreme-fire seasons has increased dramatically in many regions of the world, being associated in most cases with the effect that climate change is already posing on wildfire regimes and wildfire behaviour. Examples of these extreme wildfires were those occurring in Indonesia (2015), Chile (2016), California (USA, 2017, 2018, and 2020), Canada (2017), Portugal (2017), California (2018), Greece (2018), Australia (2019), Siberia (2019), Argentina (2021), Brazil, Bolivia, and Paraguay (2019). Common to these events was the explosive behaviour of the single fires, which resulted in the

loss of many lives and huge economic damage. Several entities reported and analysed these wildfires that interact with the atmosphere (Delicado and Gomes; Comissão Técnica Independente, 2017), increasing wind speed and causing sudden wind direction changes and local fire tornadoes (Lareau et al., 2018b; Pirsko et al., 1965) and vortexes (Khaykin et al., 2020).

Often, the fire management agencies in these countries make use of past fire history to analyse the potential behaviour of future wildfires. Fires are characterized by their rate of spread and fire intensity as well as the weather and fuel conditions when they occurred. One of the most commonly used fire danger indices is the Canadian Forest Fire Weather index (Van Wagner, 1974); this is currently used in many countries around the world and even at the global scale (Vitolo et al., 2020). Other common fire danger indices are the Australian McArthur, the US National Fire Danger Rating System (NFDRS), or the Ketch–Byram drought index. Most of these indices provide reasonable information on the potential of a wildfire to spread and cause damage. However, these indices do not evaluate the context of the atmosphere around the fire.

Wildfires are phenomena driven by fuel conditions, topography, and weather. Fuel conditions are determined by rainfall, temperature, and relative humidity among others factors. Some of these factors, such as wind and rainfall, are very dynamic in time, while others are static and characterize the local fire behaviour, such as topography. The behaviour of extreme fires, which prevents the evacuation of the affected areas and the possibility of fire extinction, is often related to the interaction of the wildfire dynamics and the conditions of the atmosphere around it (also known as coupled effects). There are multiple factors that define the fire spread behaviour. The relevance of a given factor as the most important or dominant for the spread sometimes defines the type of fire. One single fire event may transition from one type to another. For instance, examples of these types are fuel-dominated fires or wind-driven fires. In this work we will refer to fire driven by convection when convection is an important driving factor of the fire spread.

A first approximation to take into account regarding the atmospheric instability around wildfires was the Haines Index (Haines and Service, 1988), which is usually computed between two different heights of the atmosphere above the fire. In cases of extreme-wildfire events, the Haines Index (Potter, 2018a) can identify dangerous fire spread conditions by using values of temperature and humidity at different elevations. Although the index was successfully used in large fire episodes in the USA (Potter, 2018b), it failed to explain or predict the behaviour of extreme fires that have happened recently (Pinto et al., 2020).

The main objective of our work is to evaluate the proposed fire danger index (extreme-fire behaviour index, EFBI), which considers deep moist convection, as this is not usually taken into account in most traditional fire danger rating indices applied at the global scale.

In some cases, the Haines Index saturates (Potter, 2018a), remaining at its maximum value, as in the case of the fire in Pedrógão Grande, Portugal, in 2017 (San-Miguel-Ayanz et al., 2019). The aim of the EFBI is to summarize the factors that may imply a change in fire behaviour and to determine how easy it is for the change in fire behaviour to happen. Several authors used factors for storm forecasting such as the convective available potential energy (CAPE) and convective inhibition (CIN) to address fire behaviour (Moncrieff and Miller, 1976). Conditioned atmosphere stability was often a common factor of extreme-wildfire events. Consequently, increasing the temperature and/or humidity at the surface could lead to atmospheric instability, causing local, dangerous, and unexpected conditions.

Wildfire behaviour can be modelled by forest fire simulators, which provide a forecast of the fire intensity and spread. These simulators are based on semi-empirical (Rothermel, 1972) or physical (Mell et al., 2007) models and can be coupled with atmospheric simulation models (WRF-Fire, Weather Research and Forecasting, Mandel et al., 2011; ForeFire–Meso-NH, mesoscale non-hydrostatic, Baptiste Filippi et al., 2009) or wind field production models such as WindNinja (Forthofer et al., 2009) to assess wildfire behaviour. However, as the numbers of coupled models grow, the simulation becomes computationally more expensive, and it is difficult to gather the required input data without strong uncertainties. Therefore, fire danger ratings and the experience of meteorologists, civil protection officers, and fire analysts play an important role in decision making. Moreover, it is not feasible to use coupled models for simulating all wildfires detected at the global scale. The capacity to forecast the conditions under which these critical fires can develop is thus of paramount importance and essential for the prevention of damage to the population and human assets. We hereby present a fire danger index referred to as the extreme-fire behaviour index (EFBI), which looks into the ease of interaction of the wildfire dynamics with the surrounding atmosphere, targeting deep moist convection, and determines if the behaviour of an ignited fire can become critical, allowing it to develop into an extreme wildfire (Duane et al., 2021). The size distribution of the fire events is unbalanced, being more common in small-size fires with an expected fire spread speed. Although less frequent, there is a set of fire events with high fire spread that overwhelms firefighting capabilities and reaches larger amounts of burnt area. A subset of these fires, considered extreme fires, interact with the atmosphere around them, leading to unexpected or erratic behaviour. Among these extremes fires, some are characterized by the occurrence of pyrocumulus (pyroCu) and pyrocumulonimbus (pyroCb) clouds, analysed in Lareau and Clements (2016). The occurrences of these phenomena led to works that analysed the pyrocumulus (Tory et al., 2018) clouds and to the assessment of the potential of pyroconvec-

tion (Leach and Gibson, 2021; Tory and Kepert, 2021) using different approaches, for instance, including the moisture and heat released by the fire (Potter, 2005). In the last decades the amount of extreme fires has become very relevant, and it has increased awareness about fires as dangerous natural hazards. Besides, the relation of climate change with those events has been studied (Di Virgilio et al., 2019) relying on regional records (McRae et al., 2015) (for Australia) and using well-known fire danger indices such as the McArthur Forest Fire Danger Index (FFDI) (McArthur, 1967) and Haines Index (Haines and Service, 1988). At the global scale, the existing records of fire data are quite fragmented, and there is much more uncertainty when compared to using methods and data suitable for specific regions as mentioned in fire-related studies at the global scale such as Bowman et al. (2017).

We used a global wildfire database (GlobFire; Artés et al., 2019) and ERA5 weather reanalysis data (Hersbach, 2016) to compute the EFBI over a set of wildfires. Our approach is suited to being computed at the global scale using operational weather forecast models to determine when an ongoing fire can develop extreme-wildfire behaviour due to deep moist convection. First, Sect. 2 describes the proposed index, the workflow for wildfire event selection from the global wildfire database and the retrieval of the meteorological data, and the description of three study cases. The results of the EFBI for the study cases are explained in Sect. 3. Finally, the conclusions are presented in Sect. 4.

2 Data and methods

The proposed EFBI relies on the premise that the atmosphere can cause a wildfire to be and become convection driven or that the wildfire can disrupt the atmosphere, creating a convective trend. The EFBI is based on well-known indicators of convection such as Eqs. (2) and (3), which are also used in Potter (2005) to demonstrate the effects of the increased moisture due to the water released during the fire combustion or the warmed air at the ground surface. In addition Lareau and Clements (2016) measured and analysed atmospheric data, using lidar and radar, to study pyroCu and pyroCb. Lareau and Clements (2016) showed how the plume condensation level is higher than the ambient lifting condensation level (LCL). Besides, they suggested using the convective condensation level (CCL) for estimation of the convective temperature for a best representation of the plume condensation level. Also, Tory et al. (2018) proposed a method to estimate the firepower threshold required for pyroCb potential. Leach and Gibson (2021) proposed a parcel-based model to assess how the atmosphere will affect a growing wildfire plume, including heat and moisture released from the fire. In this work we propose a method which computes the current convection trend of the atmosphere using CAPE and CIN, then estimates the temperature required to have a CIN $>= 0$ in the parcel, also known as convective temperature, which

can be obtained when computing the CCL. Finally, we compute the convective energy difference between the modified profile and the original one. Most of the past works were based on data gathered on the field, study cases, or a database classified as potential pyroCu or pyroCb (as in Di Virgilio et al., 2019). In this case, we do not estimate the heat and the water release of the fire (as in Leach and Gibson, 2021), but we evaluate the information contribution from a relatively simple approach to estimate moist convection, which is feasible to be applied with global weather forecasts. Therefore, we assume that the difference between the surface temperature and the convective temperature is a potential indicator of a change in potential convective energy and can trigger the change in fire behaviour. More physically detailed approaches have been proposed like the blowup (BU) ΔT term in Leach and Gibson (2021), and the ΔT_f term of Tory et al. (2018) has been proposed for pyroCb–pyroCu assessment or plume dynamics, but they cannot be analysed at the global scale with the available open datasets.

The extreme-fire behaviour index (EFBI) determines the amount of increase in temperature at the surface required to cause a null CIN and quantifies the change in the available convective energy. The amount of change of convective energy per degree Celsius is used as indicator of ease of deep moist convection.

The EFBI is computed as follows:

$$\text{EFBI} = \frac{((\text{CAPEP} + \text{CINP}) - (\text{CAPE} + \text{CIN}))}{\Delta T}, \quad (1)$$

$$\text{CAPE} = \int_{Z_f}^{Z_n} g \frac{(T_{v,\text{parcel}} - T_{v,\text{env}})}{T_{v,\text{env}}} dz, \quad (2)$$

$$\text{CIN} = \int_{Z_{\text{bottom}}}^{Z_f} g \frac{(T_{v,\text{parcel}} - T_{v,\text{env}})}{T_{v,\text{env}}} dz, \quad (3)$$

$$\{\Delta T \in \mathbb{R} | (\Delta T = T_{\text{bottomConv}} - T_{\text{bottom}}) \wedge \text{CIN} \geq 0$$
$$\wedge \Delta T \geq 0\}, \quad (4)$$

where CAPE and CIN are defined by Eqs. (2) and (3) (Moncrieff and Miller, 1976; Williams and Renno, 1993) and ΔT is the change in temperature degrees required to achieve a null or negative convective inhibition energy (CIN) (Eq. 4). ΔT is obtained from the difference between the surface temperature and the increased temperature. The increased temperature is obtained from the CCL as stated in Lareau and Clements (2016) as a more accurate way to estimate the pyroCb–pyroCu initiation heights and implies CIN $>= 0$. CAPE and CIN are recomputed with the increased temperature ($T_{\text{bottom}} + \Delta T$) and called CAPEP and CINP, with CINP being zero or greater than zero (no inhibition). Z_n is the height of the equilibrium level; Z_f is the height of the level of free convection (LFC); g is the acceleration due to gravity; $T_{v,\text{parcel}}$ is the virtual temperature of a given parcel; $T_{v,\text{env}}$ is the virtual temperature of the environment; Z_{bottom} is the

lower height; T_{bottom} is the temperature at the lower altitude; and $T_{\mathrm{bottomConv}}$ is the temperature at the lower altitude that causes CIN $>= 0$.

In cases in which the atmosphere is already unstable, CIN is equal to or greater than zero, being $\Delta T = 0$, the values assigned to the index are the full integration of CAPE + CIN.

The EFBI is expressed in $\mathrm{J\,kg^{-1}\,°C^{-1}}$, which is the amount of energy exchange per unit of mass and per degree of temperature. The value can be used as an estimation of potential wildfire–atmosphere interaction.

High EFBI values point to a sudden change of energy per mass for a small temperature increase (low value of ΔT and high value of total convective energy). Under these conditions, air can potentially move vertically, creating local conditions which are not explicitly provided by meteorological forecasts. When the values are low, the magnitude of the change is small, and/or a higher temperature is required at the surface to cause any change. This information is essential for firefighters, since local eddies and sudden weather changes can occur and lead to very fast ember-spotting fire spread, which creates dangerous and unpredictable conditions for front line safety (Lareau et al., 2018a).

To test the EFBI, we propose two machine learning approaches, a decision tree and a multilayer perceptron. The EFBI and Canadian Forest Fire Weather index (FWI) were used to evaluate the discriminatory potential between two fire classes: small fires (500 ha during more than 1 d) and large fires (10 000 ha in 1 d). Fire events were extracted from the GlobFire database. The fire size thresholds were chosen to consider both average and extreme-fire spread. Small-size fires were selected in the same zones where the large fires were selected but in a different year and always outside the area burnt by the large fires. Using the same zone for both sets of fires, we limited the variability in fuel and topography, ensuring that the differences in fire behaviour were due to the meteorological conditions under which the fires evolved. Often small fires are caused by fire spotting or as the result of agricultural practices. To avoid these types of fires, it was required that the fires had more than 90 % of the burnt area in wildland vegetation. The final selection was a total of 445 cases, with 223 fires larger than 10 000 ha and 222 fires smaller than 500 ha. Figure 1 shows the distribution and the year of each fire at the global scale.

For each fire, the Canadian Forest Fire Weather index (FWI) and all its components were retrieved from the ECMWF ERA5 dataset at 0.25° resolution (Vitolo et al., 2020). In order to differentiate between agricultural fires or wildfires, the land cover from the Climate Change Initiative (CCI; Defourny et al., 2012) was used, requiring that 90 % of the burnt area was forest or shrubs and thus avoiding fires in crops or agricultural areas. For each selected fire, temperature, relative humidity, and wind profile were retrieved for all the heights above the wildfire event using the application programming interface (API) of the Climate Data Store (CDS) for the ERA5 reanalysis dataset (Hersbach, 2016). Then, the

EFBI and the vertical profiles for every event were computed, producing skew-t plots for every time step and generating plots with the time evolution of the index and the factors used for the computation of the EFBI. The aim of the skew-t plots is to visualize the ease with which the fire may become convection driven given an atmosphere context.

All the parameters obtained from the FWI and EFBI were used to compute the mutual information (MI) of the wildfires that spread more than 10 000 ha in 1 d (large) or less than 500 ha in more than 1 d (small). The MI has been chosen to quantify the individual importance of the variables gathered for each fire (such as the FWI components and the EFBI) in relation to the speed of the spread of the fire, which is categorized into either small- or large-fire events. The FWI was computed for an entire day, and the EFBI was computed with 1 h time steps. Therefore, the values of the EFBI were aggregated using the minimum, the maximum, and the average value for the time window. In addition, the date associated with the burnt area was based on GlobFire, which uses the burnt area product of MODIS MCD64A1 (Giglio et al., 2015). Due to clouds or dense smoke plumes, it is possible that a fire might have not been detected until some days after its ignition. To account for this delay, the initial day of the time window for the FWI and EFBI was decreased by 2 d. The maximum value of the FWI and its components during the time window were selected. When applying the FWI at the global scale its values are not comparable between different locations. Despite that fact, the percentiles of the FWI can provide information about the fire danger for a given area. Therefore, the values of the FWI were used in percentile values, computed for the period 1979 to 2019 of the same week of the year.

In addition to the proposed EFBI and FWI, cHaines (continuous Haines Index) is also computed using the same ERA5 data used for the EFBI. For the temperature depression term, we used the temperature at 850 and 700 hPa. For the dew point depression term, we used temperature at 850 hPa and dew point temperature at 850 hPa.

The MI for continuous values was computed using the method described in Kraskov et al. (2004) and Ross (2014) and using Pedregosa et al. (2011). These methods use a nearest-neighbour approach with a random initialization; for that reason, 10 additional attributes were added to the analysis with random values to evaluate the noise of the MI. The MI computation was done 1000 times. The computations of the MI were initialized with random values to evaluate the noise of the attributes for the MI computation.

In addition, the behaviour of the EFBI was shown analysed for three different study cases. First, we analysed the fire in Pedrógão Grande, Portugal, in 2017 using high-spatial- and high-temporal-resolution fire perimeters. Next, the EFBI was computed with forecast data using for the analysis the daily fire perimeters of the wildfire that took place in Roboré, Bolivia, in 2019. Lastly, we studied the spatial distribution of
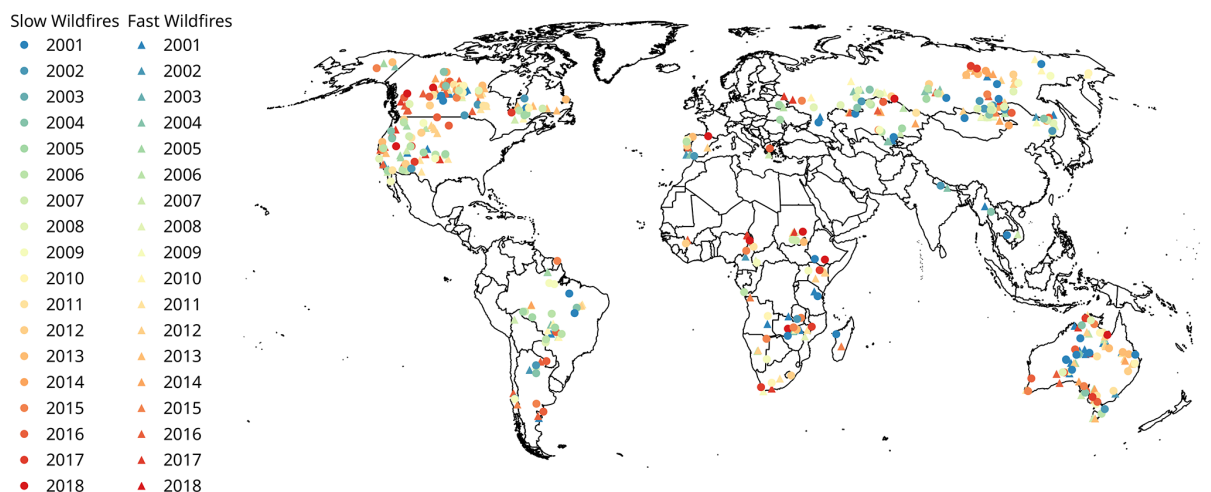
Figure 1. Location of the wildfires coloured by year. Fast fires and slow fires are depicted with triangles and circles respectively.

the EFBI for the set of extreme wildfires in the southeastern coast of Australia at the end of 2019.

3 Results

EFBI results are evaluated by combining the resulting values of the EFBI and FWI (Vitolo et al., 2020) to predict extreme-fire behaviour observed in GlobFire using weather data from ERA5 (Hersbach, 2016). In this work, a machine learning approach is used to check the feasibility of using the EFBI to predict extreme-wildfire behaviour at the global scale. In addition, the EFBI values are shown for several study cases.

In Fig. 2, we illustrate how EFBI components behave for a given vertical profile at a given time step. The blue area is the convective inhibition (CIN), and the red area (from the point for the level of free convection (LFC) to the equilibrium level (EL)) is the convective available energy (CAPE). When CIN values are low and CAPE values are high, wildfires can be convection driven at high altitudes. A temperature increase at the surface can reduce CIN values and increase CAPE values. Figure 2 shows a skew-t plot with the parameters used to compute the EFBI. The figure shows the vertical profile of the atmosphere with the temperature as a red line and the temperature dew point in green at different altitudes (right vertical axis). These parameters are enough to compute the amount of work caused by the buoyancy force. By modifying temperature and dew point temperature the buoyancy changes and, consequently, the trend of the air to move. Figure 2 shows how a change of $14\,°C$ at the surface temperature causes a considerable change in CAPE and CIN values with a CAPEP close to $2443\,\mathrm{J\,kg^{-1}}$ and a low value of CINP. The temperature increase, $14\,°C$, is only used, as is an indicator of the moist-convection trend by an increase of heat at the surface, since the biomass burnt, heat, and gases released by the fire are not estimated; the heat dissipation is not

simulated or estimated (Byram, 1954; Morvan and Frangieh, 2018; Tory and Kepert, 2021). Therefore, the amount of work due to the buoyancy change passes from $34\,\mathrm{J\,kg^{-1}}$ (CAPE) to $2443\,\mathrm{J\,kg^{-1}}$ (CAPEP) when CIN is not an inhibition, i.e. passing from a negative value to a positive value. This leads to a total change of $233.531\,\mathrm{J\,kg^{-1}\,°C^{-1}}$ for each degree increase at the surface. The CAPEP is around $2443\,\mathrm{J\,kg^{-1}}$ when thunderstorms often exceed CAPE values of 1000 and $5000\,\mathrm{J\,kg^{-1}}$ in extreme cases (Lombardo and Colle, 2011). The increased temperature (ΔT) can not be understood as a real temperature increase but as an indicator, since it would not be realistic that an entire parcel receives enough energy to increase the surface temperature instantly being isolated from the neighbouring parcels and upper layers. In this work, we assume that the EFBI can be an indicator of ease of deep moist convection, but we do not take into account all complex factors involved in fire behaviour and atmosphere interactions (Sullivan, 2017). Figure 2 also illustrates how the CCL is used as suggested by Lareau and Clements (2016) as a better estimation of the convective temperature for a best representation of the plume condensation level. From the CCL temperature, following the dry adiabatic up to the surface, we obtain the temperature which would neutralize CIN and increase considerably CAPE.

It is worth mentioning that CIN values at lower heights are also related to the temperature dew point at the surface (green line at 1000 hPa). With a constant temperature at the surface and an increase of dew point temperature, the CIN is reduced, and therefore the EFBI increases. This may happen with a sudden increase of humidity at the surface, without any increase of temperature (already taken into account in the computation of the EFBI).

The timeline of the EFBI for the wildfire in Sala (2014, Sweden) is shown in Fig. 3. The time period when the fire had an extreme behaviour, as documented by firefighters on the ground, is delimited with vertical dashed lines. In
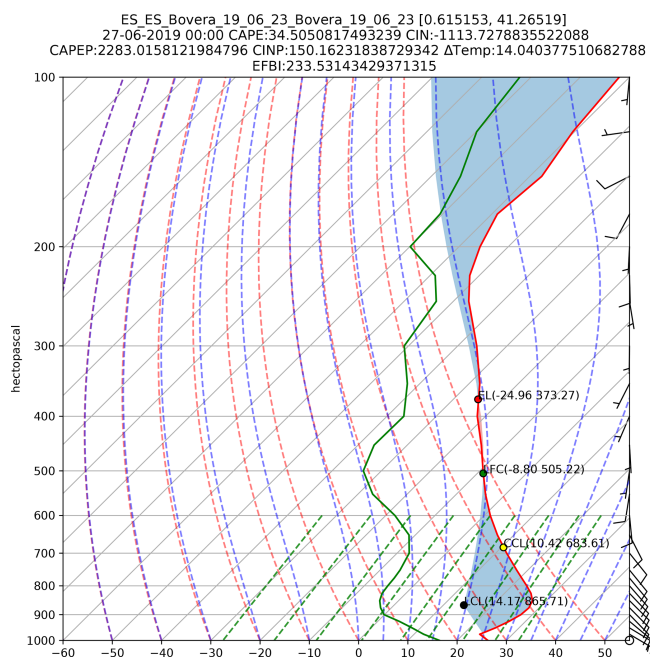
ES_ES_Bovera_19_06_23_Bovera_19_06_23 [0.615153, 41.26519]
27-06-2019 00:00 CAPE:34.5050817493239 CIN:-1113.7278835522088
CAPEP:2283.0158121984796 CINP:150.16231838729342 ΔTemp:14.040377510682788
EFBI:233.53143429371315

Figure 2. Sample of one skew-t plot for a given time step for the wildfire that took place in La Torre de l'Espanyol, Spain, and burnt 6625 ha from 26 to 27 June 2019.

this period, the modified convective available energy reaches values above $2500\,\mathrm{J\,kg^{-1}}$, and the index values are near $800\,\mathrm{J\,kg^{-1}\,{}^\circ C^{-1}}$.

The EFBI is computed for each time step, as explained in the previous illustrative example, for all the cases extracted from GlobFire database using the method described in Sect. 2. Regarding the information of the different features used to discriminate small from large fires, Fig. 4 shows the values of the MI mean and standard deviations of each attribute for the 1000 iterations. The use of only the minimum, maximum, or average of the EFBI provided more information to separate small from large fires than the percentile and value of the drought code (DC) of the FWI. Figure 4 does not show the discriminatory power of all variables but rather the amount of information with which each of the factors individually contributes to the classification between the two classes. The EFBI on its own cannot easily discriminate between the classes without using factors included in the computation of the FWI such as fine fuel moisture content (FFMC), duff moisture code (DMC), or drought code (DC). The discriminatory potential between the two classes using the EFBI is very low without using the FWI. Regarding the MI of cHaines, the minimum value provides a considerable amount of information, more than the minimum value of the EFBI. However, the maximum value of cHaines provides a very low amount of information when compared to the maximum value of the EFBI, which provides valuable information for the classification. That fact could point to a potential saturation of cHaines, meaning that the maximum

value is not giving information about whether the fire is small or large.

For instance, the EFBI can have high values after a rainfall event. It is thus important to stress that the EFBI becomes relevant when combined with the FWI components. A decision tree based on information gain as the criteria was used to show the relevance of the EFBI in discriminating small fires from large fires. Figure 5 shows the decision tree, which is based on entropy reduction with a maximum depth of four levels (for visualizing purposes). The root uses the daily severity rating (DSR), which is a transformation of the FWI. At the second level, the maximum value of the EFBI is used, before considering any of the FWI components such as the percentiles of the initial spread index (ISI), the drought code (DC), the built-up index (BUI), and the fine fuel moisture content (FFMC). Therefore, the EFBI helps to reduce the entropy when discriminating between the two classes at the global scale, being more relevant than the ISI or DC percentile.

A machine learning approach was applied using a decision tree and a multilayer perceptron. Removing the maximum depth restriction to the decision tree and performing a cross-validation of 1000 splits with 5 % of cases, as a test, the average accuracy was 65.13 % with a standard error of 7.29 %. The accuracy was computed using scikit-learn considering the accuracy of the percentage of each sample with which each label is correctly predicted.

Applying a multilayer perceptron with 3 hidden layers of 300 neurons each with ReLU (rectified linear unit) activation and using an Adam solver (KingaD, 2015) optimizer for training and the same parameters for a cross-validation, an accuracy of 78.37 % (standard error of 1.85 %) was reached. If the parameters related to the FWI were exclusively used, the accuracy decreased to 60.75 % (standard error of 2.24 %). Using FWI with cHaines raised the accuracy to 63.42 % (standard error of 4.12 %). All input values have been normalized for the three cases (FWI, FWI + EFBI, and FWI + cHaines).

As previously mentioned in Sect. 2, the dataset used to test the EFBI was obtained using a fully automated process. The information regarding the fire behaviour was obtained from GlobFire using SQL (Structured Query Language) queries. The query guarantees that there are no fires happening in a 2° radius around a detected fire during a time period of 30 d. During the cross-validation process, the wildfires that were more frequently misclassified can be identified. When looking at the first 50 wildfires that are often misclassified, the proportion of the cases is very balanced between true small- and large-fire cases. Assuming that such cases are a source of noise and can be deleted from the dataset, the accuracy rises to 80.30 % (standard error of 1.94 %). It should be noted that some cases could be false positives or false negatives. False positives could happen when a fire was burning in a cloudy area for several days. Once the area is free of clouds, the burnt area is detected for that day, even it was
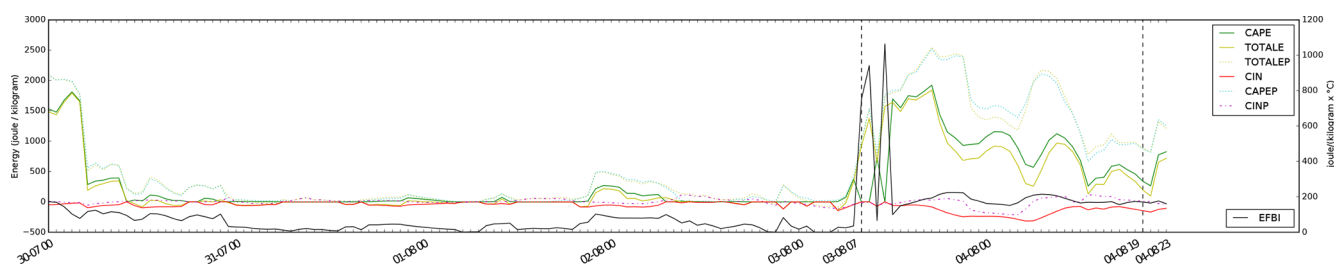
Figure 3. Sample of the timeline of the EFBI (right vertical axis) and the factors used (left vertical axis) for the wildfire in Sala (2014, Sweden) that burnt close to 10 000 ha from 3 to 4 August 2014 (time period marked with vertical dashed lines). Horizontal axis is the timeline using hourly steps in the format dd-mm hh. TOTALE = CIN + CAPE. TOTALEP = CINP + CAPEP.
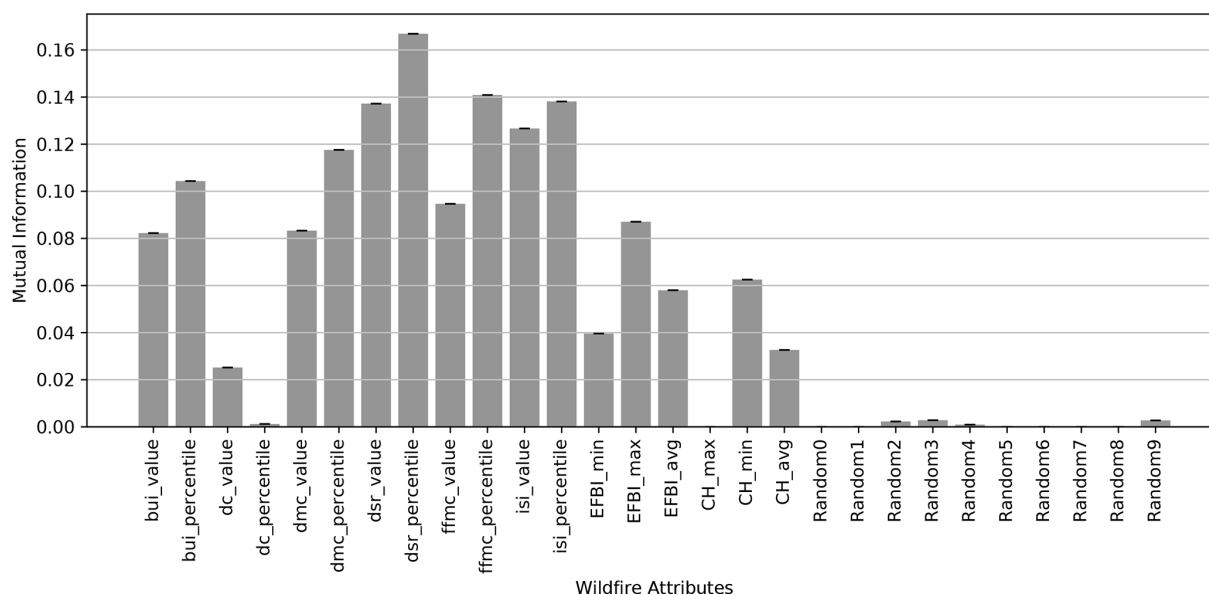

Figure 4. Mutual information of the different attributes gathered for each fire regarding their tag as fast or slow fires. CH: cHaines.

burning for days before this day. False negatives may have happened with re-ignitions of large fires. Besides, large fires are not always convection driven or related to an unstable atmosphere. The current automated process to discriminate potential large fires using the GlobFire database can be implemented in near-real time, using weather forecast data, allowing for the potential identification of dangerous convection-driven fires in advance and thus increasing the wildfire danger rating. This, in turn, would increase preparedness for firefighting procedures and enhance the safety of crews on the ground. Additionally, the overall procedure in the discrimination of potential large fires can be improved if the dataset is manually checked and the fire types are better defined.

3.1 Study cases

3.1.1 Pedrógão Grande, Portugal, 2017

This wildfire had one of the most severe fire behaviours in Europe. The fire was ignited on 17 June and ran until 23 June.

Figure 6 shows an explosive expansion from 17 to 18 June, which is followed by a constant but severe fire expansion. For this analysis the fire perimeters made for a wildfire report done by a technical commission (Comissão Técnica Independente, 2017) were used as reference for the fire spread.

From 17 to 18 June there was an increase of burnt area larger than 20 000 ha in 1 d.

Figure 7 shows the value of the EFBI and its components during the entire month for the fires computed from the ERA5 reanalysis; the two vertical dashed lines in the figure delimit the duration of the fire. The EFBI shows that there is a considerable potential for the interaction of the fire with the atmosphere. In addition, during the days of the fire there was a natural CAPE of nearly 5000 $J\,kg^{-1}$ inhibited by a small value of CIN. Increasing the temperature at the surface, removing the inhibition, would produce a sudden convection. The index values are close to a 250 $J\,kg^{-1}\,°C^{-1}$ increase and a total convective energy about 6000 $J\,kg^{-1}$.

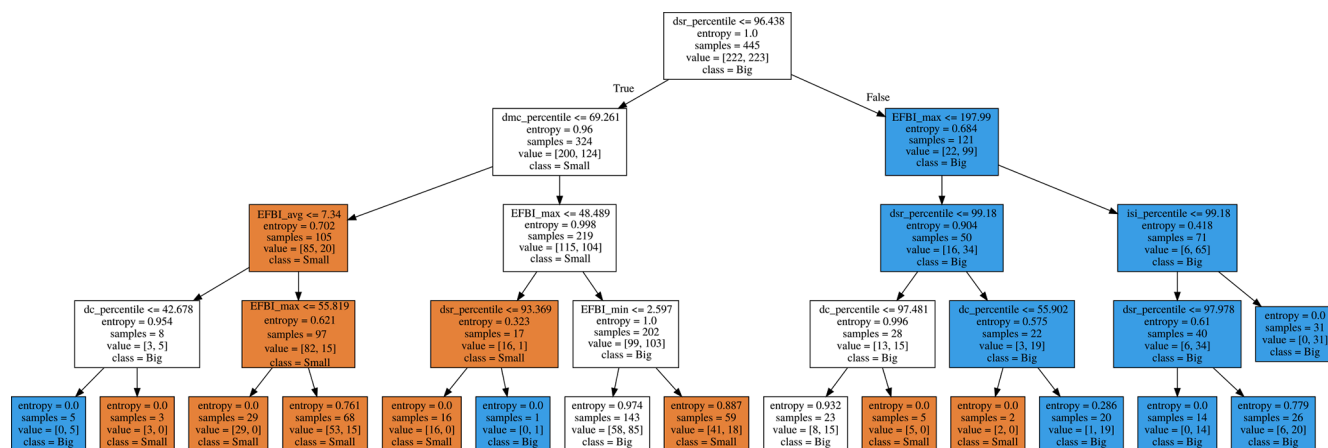This case shows a natural tendency towards a convection-driven behaviour that may be caused by the atmospheric in-

Figure 5. Decision tree based on entropy reduction built with the 445 wildfire events (222 small and 223 large wildfires).
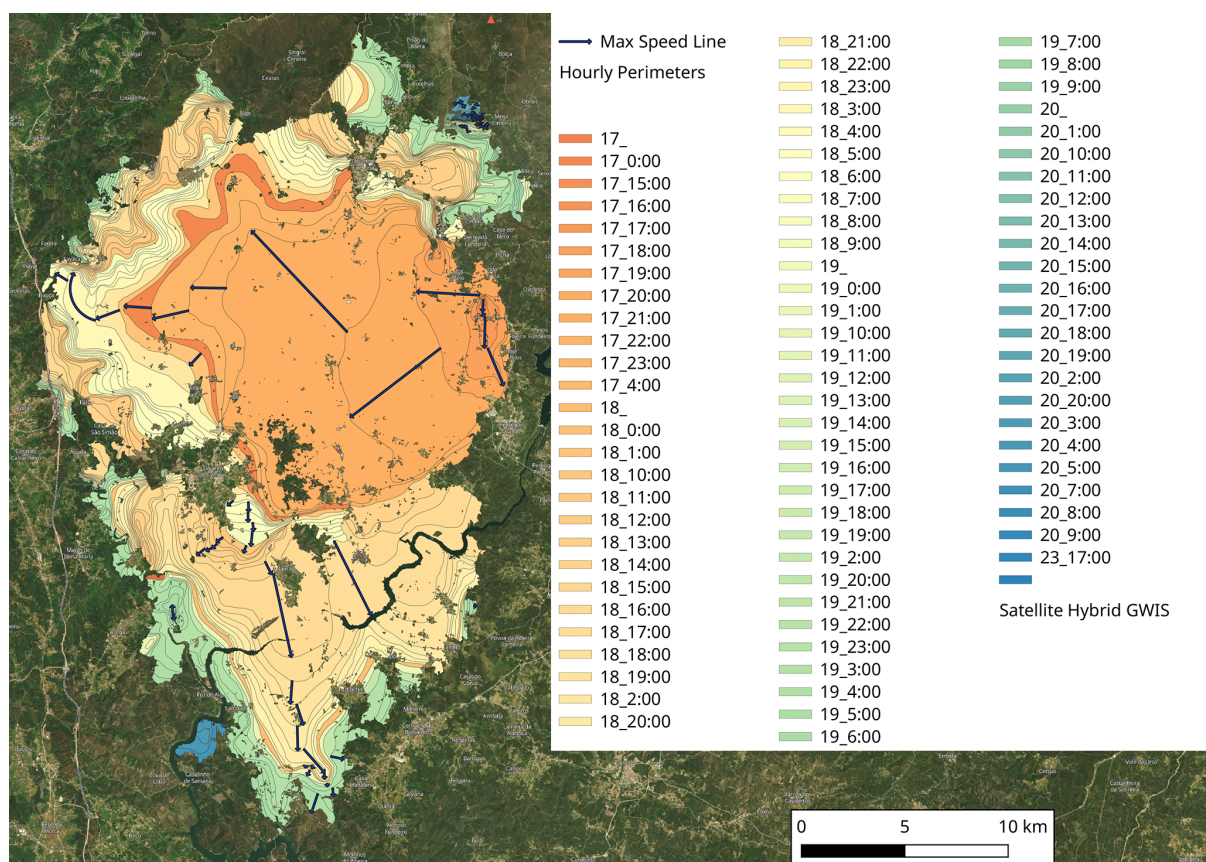

Figure 6. Time sequence of the wildfire which took place in Pedrógão Grande (Comissão Técnica Independente, 2017), Portugal, on 17 June 2017. The maximum speed line between time steps is shown with a black arrow. Background image © MapTiler (https://maptiler.com/copyright, last access: 15 March 2021). GWIS: Global Wildfire Information System.

stability itself, without the need for a considerable amount of heat and/or an increase in relative humidity at the surface.

For this case study, detailed fire perimeters for each time step were available, which made it possible to analyse the relation between the maximum fire spread and the EFBI. Fig-

ure 8 shows a scatter plot where each point is a time step given an EFBI value and the estimated maximum fire speed. While a wide variety of values of the EFBI are shown for low fire spread speed values, considerably higher EFBI values are shown for high speed values, compared with the rest of the
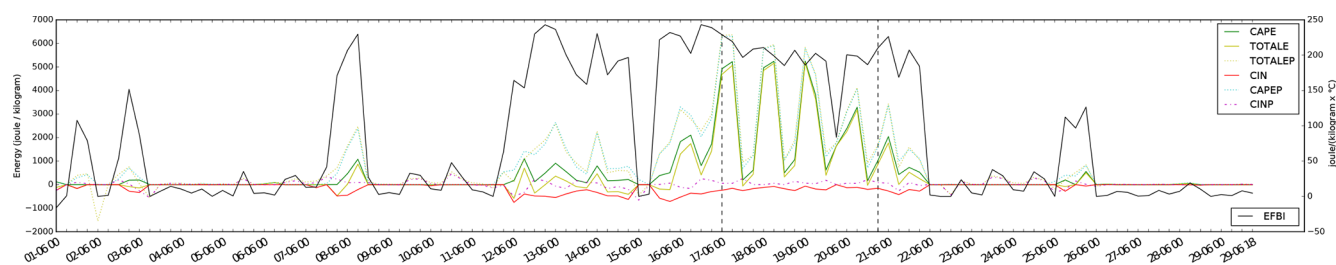
Figure 7. The EFBI and its components for the wildfire in Pedrógão Grande on June 2017 for the fire centroid (-8.2252, 39.952). Horizontal axis is the timeline using hourly steps in the format dd-mm hh.
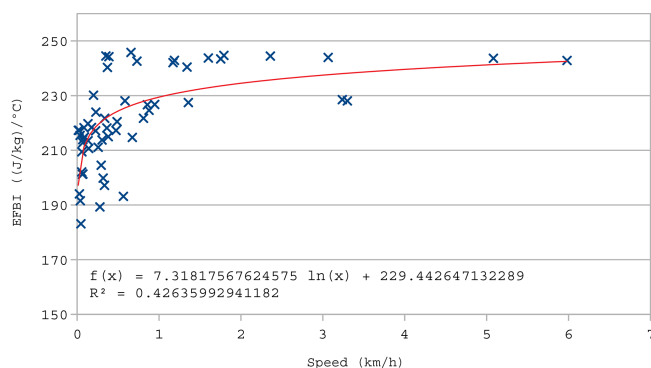

Figure 8. Scatter plot showing the maximum fire front speed and the values of the EFBI for each time step with a logarithmic trend line.

point cloud. However, there is a weak correlation between the speed and the EFBI. It is worth mentioning that the blowup of the wildfire took place at the beginning of the event; assuming that the fire was in convection almost from the first time steps, the EFBI and fire spread speed may not show a strong correlation when looking at all the hourly time steps. However, Fig. 8 shows that, even with an ongoing convection-driven fire, the atmosphere stability context computed from a numeric model is still important, and speeds faster $1 \, \text{km} \, \text{h}^{-1}$ are only present when the EFBI is above 220.

3.1.2 Forecast use in Roboré, Bolivia, 2019

The values of the EFBI were computed using the ERA5 forecast for the fire that took place in Roboré, Bolivia, in 2019. This wildfire lasted 2 months and had a very variable fire behaviour. Figure 9 shows the daily burnt area for this wildfire using the GlobFire database. However, the level of detail of the fire mapping for this study case is not as accurate as in the previous case shown in Fig. 6.

For this case, the EFBI was computed with three different deterministic forecasts of ERA5 on 15 and 29 August and 3 September. During this wildfire, the EFBI forecasted different periods of extreme behaviour caused by moist convection, although the correlation was not as clear as in the case shown in Sect. 3.1.1. For long duration wildfires that inter-

act with the atmosphere it can be assumed that once a wildfire interacts strongly with the atmosphere, the trends of the EFBI are no longer valid, since they are based on a forecast that does not include the interaction. However, in the above case of Bolivia, our results show that, despite the wildfire–atmosphere interactions, the overall moist convective trend may remain important and the values of the EFBI can be relevant for a second convection interaction. It is not feasible to find a correlation between the fire spread and the EFBI values in this case because the quality of the fire mapping is daily, with a potential uncertainty of days of the maps. Also, the weather forecast that has been computed previous to a potential wildfire–atmosphere interaction may not depict the atmosphere around the fire just after a wildfire–atmosphere interaction.

Figure 10 shows the computation of the daily EFBI average joining the data from the different forecasts. In addition, the GlobFire database was retrieved and used to estimate the maximum daily fire run. Since the daily burnt area could have been mapped with some days of delay, an average was applied to the maximum daily fire run using a time window of the 2 previous days. Figure 10 shows a peak of the EFBI followed by another one which started on 16 August and a third peak on 22 August. After the first peak, the maximum fire longitude of the daily burnt areas had increased from 16 to 20 August, while the highest runs of the fire happened between 18 and 20 August; the fire activity has another peak after 22 August, having two observed pyroCb clouds on 18 and 25 August. After 25 August, the EFBI trends seem to be totally uncorrelated with the fire runs until 1 September. Afterwards, there is another peak on 7 September which also seems to affect the fire runs, with two observed pyroCb clouds on 7 and 8 September. Later, the EFBI and the maximum line length are again uncorrelated until 17 September when there is again a relation at the last peak of the run, when another pyroCb was observed.

An example of a pyroCb seen with Sentinel-2 is displayed in Fig. 11, where parts of the plume are shown in white.
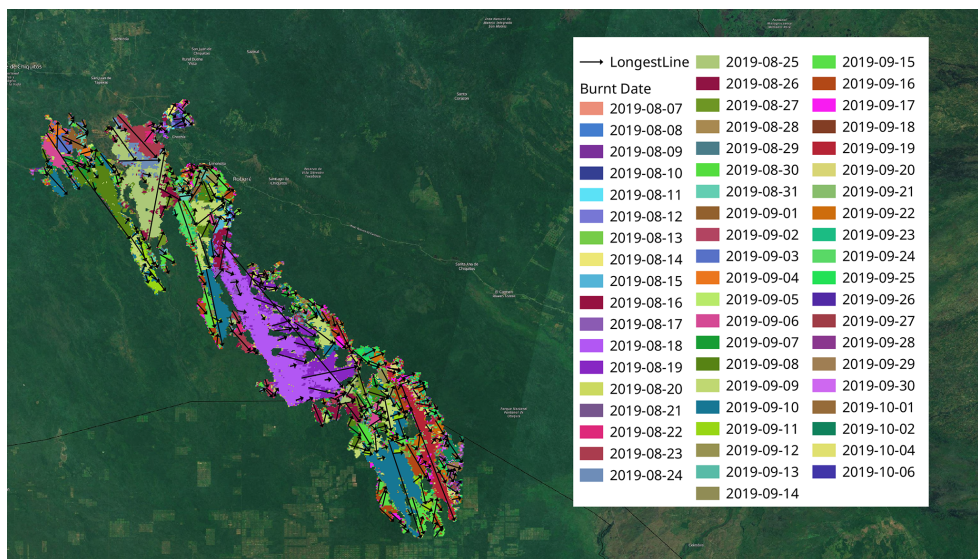
Figure 9. Daily burnt area for the duration of wildfire in Roboré, Bolivia, in 2019. The maximum speed line between time steps is shown with a black arrow. The missing days do not have any daily burnt area in GlobFire. Background image © MapTiler (https://maptiler.com/copyright, last access: 18 March 2021). Please note that the date format in this figure is yyyy-mm-dd.
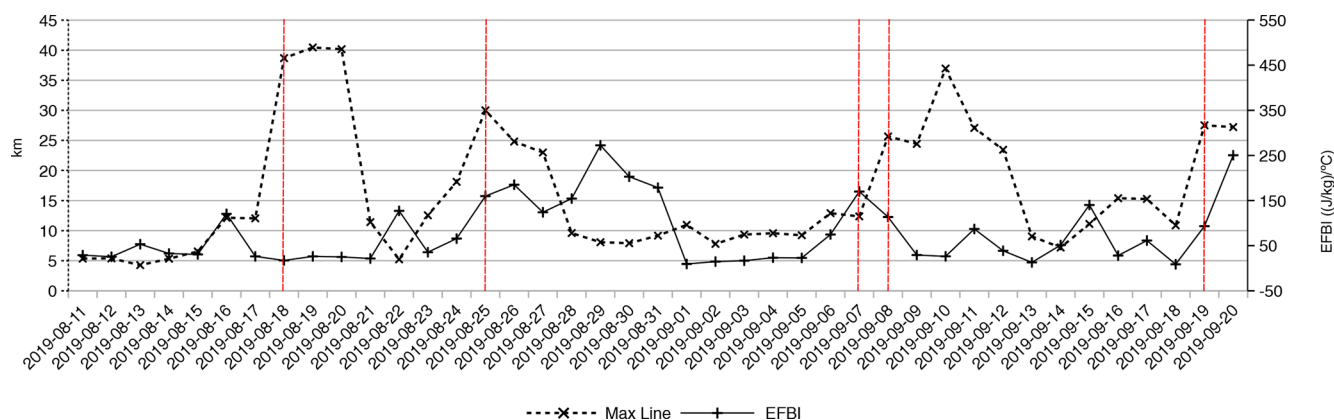
Figure 10. Maximum longitude of the daily burnt area and the EFBI and its components for the wildfire in Roboré, Bolivia, in 2019. Vertical dashed red lines show when a pyroCb took place. Please note that the date format in this figure is yyyy-mm-dd.

3.1.3 Wildfires in Australia, 2019

The EFBI was computed with ERA5 reanalysis for this area at the time of the fires showing very high values. Figure 12 shows the maximum values of the EFBI overlapped with the active fires (thermal anomalies shown as black points) that took place the next day.

It is worth mentioning that the assimilation system used to generate the ERA5 reanalysis dataset could partially affect the behaviour of the EFBI. In reanalysis, some of the consequences of heat release from the fire could be taken into account, while in the forecast for a given day those conditions would not be considered.

4 Conclusions

This work demonstrates that simple metrics of the atmosphere stability could provide valuable information for enhanced fire danger rating applied at the global scale, increasing preparedness and improving the safety and efficiency of firefighting. The EFBI could be used to detect days in which fires could exhibit extreme behaviour on a global scale. On those days, fires could add an unpredictable interaction with an atmospheric vertical profile, increasing fire behaviour due to moist convection. However, the EFBI is targeting only deep moist convection and is subject to several factors which could cause uncertainty due to the wildfire–atmosphere interaction during a forecast and to the resolution of data used. Also, convection-driven fires are not the only kind of fires
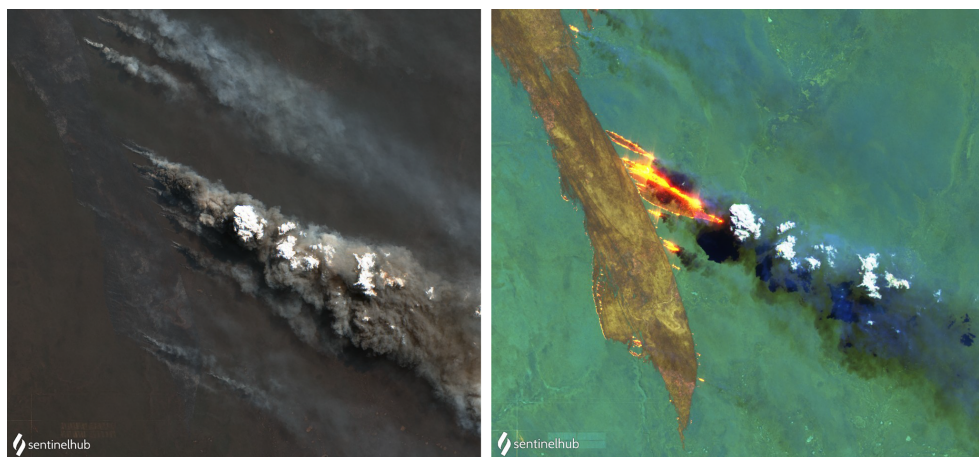
Figure 11. Sentinel-2, natural colour and atmospheric penetration, from right to left from Sentinel-2 on 18 August. Roboré, Bolivia.
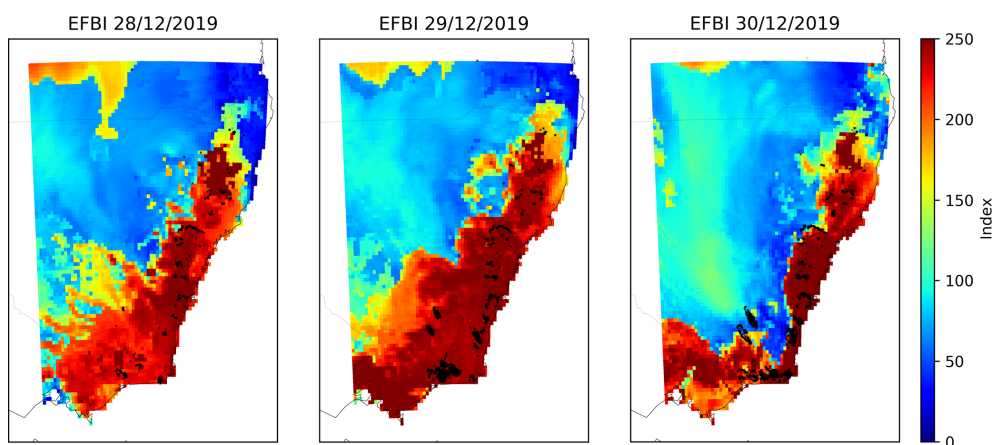

Figure 12. The EFBI from 28 to 30 December 2019 overlapped with the active fires (black dots) that took place the next day over southeastern Australia. Please note that the date format used in this figure is dd/mm/yyyy.

that can exhibit extremely fast spreading. Despite this, the approach used to differentiate between fast- and slow-spreading fires at the global scale demonstrates a potential use of the EFBI combined with the FWI to forecast extreme-fire behaviour. Moreover, the data used for the vertical profiles could be improved by estimating the surface temperature and relative humidity at the surface using the altitude of the fire even, and evaluating the air dryness at different levels.

The EFBI holds the potential to improve fire danger forecast ratings applied at the global scale. The initial testing presented in this article reached a 78 % accuracy, discriminating the final size of fires between small (≤ 500 ha) and large ($\geq 10\,000$) at the global scale. Accuracy could be improved by increasing the number of classes and using other input factors to discriminate wind-driven fires in small bushes or grass which can become large fires but have a low probability of becoming convection-driven wildfires or breaking the atmosphere stability. These big fires are not discarded in this work. For instance, dry and strong catabatic wind-driven

fires like those of the mistral (western Europe), Santa Ana and Diablo winds (California), or Zonda wind (Argentina and Chile) are not always fast wildfires caused by convection. These kinds of fires are not convection driven but are extreme fires anyway and could reduce the accuracy reached in this work. This might have influenced the study case in Roboré, Bolivia, which generated several pyroCb clouds but had also wind-driven fire spreads.

The EFBI can be computed at least twice per day at the global scale with up to a 10 d forecast. For instance, using the Global Forecast System (GFS) for a 10 d forecast at 0.25° of spatial resolution (approximately 25 km), the computation of the EFBI at the global scale took 4 h in a single node with linear speed up, using multiple cores.

The EFBI has shown high discriminatory power of large fires using ERA5 at 0.25° resolution at hourly steps and GlobFire at 500 m with a temporal resolution of 1 d. It showed a considerable relevance in the mutual information and in the discriminative power with the decision tree. It

should be noted that the training of the neural network with only FWI values and its components, which are the fire danger indices most used worldwide, dropped the accuracy from 65.5 % to 58 %. Our results also highlight the relevance of the GlobFire dataset in analysing fire behaviour and improving current danger ratings for extreme wildfires that may happen more frequently worldwide under climate change. This work also stresses the importance of developing datasets for fire behaviour, improving temporal and spatial resolution. Such datasets would enable the application and validation of complex models such as those proposed by Tory et al. (2018) and Tory and Kepert (2021) and use of detailed analysis as done, for instance, by Lareau et al. (2018a) and Bagley and Clements (2021).

Using a high-spatial- and high-temporal-resolution dataset in the study case of Pedrógão Grande in Portugal, the EFBI showed a close relation with the speed of fire spread. Moreover, using the daily data of GlobFire for the fire behaviour in the case of Roboré, the EFBI could have forecasted the convective periods during the wildfire. For the last study case, which includes a cluster of extreme wildfires in Australia, high values of the EFBI match spatially with the occurrences of such events, although the behaviour of the individual fires within the cluster was not analysed.

The above results indicate that the EFBI shows a potential to improve the current fire danger rating at the global scale by establishing a fire typology which could characterize potential explosive behaviour of wildfires using an estimation of deep moist convection and ERA5.

References

Artés, T., Oom, D., De Rigo, D., Durrant, T. H., Maianti, P., Libertà, G., and San-Miguel-Ayanz, J.: A global wildfire dataset for the analysis of fire regimes and fire behaviour, Scientific Data, 6, 1–11, 2019.

Bagley, R. B. and Clements, C. B.: Extreme fire weather associated with nocturnal drying in elevated coastal terrain of California, Mon. Weather Rev., 149, 2497–2511, 2021.

Balch, J., Bradley, B., Abatzoglou, J., Nagy, R., Fusco, E., and Mahood, A.: Human-started wildfires expand the fire niche across the United States, P. Natl. Acad. Sci. USA, 114, 2–946, 2017.

Baptiste Filippi, J., Bosseur, F., Mari, C., Lac, C., Le Moigne, P., Cuenot, B., Veynante, D., Cariolle, D., and Balbi, J.-H.: Coupled atmosphere-wildland fire modelling, J. Adv. Model. Earth Sy., 1, 11, https://doi.org/10.3894/JAMES.2009.1.11, 2009.

Boschetti, L., Roy, D. P., Giglio, L., Huang, H., Zubkova, M., and Humber, M. L.: Global validation of the collection 6 MODIS burned area product, Remote Sens. Environ., 235, 111490, https://doi.org/10.1016/j.rse.2019.111490, 2019.

Bowman, D. M., Williamson, G. J., Abatzoglou, J. T., Kolden, C. A., Cochrane, M. A., and Smith, A. M.: Human exposure and sensitivity to globally extreme wildfire events, Nature Ecology & Evolution, 1, 1–6, 2017.

Byram, G. M.: Atmospheric conditions related to blowup fires. Station Paper SE-SP-35, Asheville, NC: USDA-Forest Service, Southeastern Forest Experiment Station. 35, 1–36, https://www.fs.usda.gov/treesearch/pubs/45778 (last access: 11 February 2022), 1954.

Comissão Técnica Independente: Análise e apuramento dos factos relativos aos incêndios que ocorreram em Pedrógão Grande, Castanheira de Pêra, Ansião, Alvaiázere, Figueiró dos Vinhos, Arganil, Góis, Penela, Pampilhosa da Serra, Oleiros e Sertã entre 17 e 24 de junho de 2017, Comissão Técnica Independente, Assembleia da Répública, Lisboa, https://www.esquerda.net/sites/default/files/relatoriocti12out2017.pdf (last access: 10 February 2022), 2017.

Deeming, J. E., Burgan, R. E., and Cohen, J. D.: 1977. The national fire-danger rating system, 1978 (Vol. 39), Department of Agriculture, Forest Service, Intermountain Forest and Range Experiment Station, 1977.

Defourny, P., Kirches, G., Brockmann, C., Boettcher, M., Peters, M., Bontemps, S., Lamarche, C., Schlerf, M., and Santoro, M.: Land cover CCI, Product User Guide Version, 2, https://www.esa-landcover-cci.org/?q=webfm_send/84 (last access: 11 February 2022), 2012.

Delicado, N. T. S. and Gomes, A.: O GRANDE INCÊNDIO FLORESTAL DE PEDROGÃO GRANDE Análise Crítica, https://www.researchgate.net/profile/Nuno-Delicado/publication/319839493_O_Grande_Incendio_Florestal,

_de_Pedrogao_Grande/links/59bd712ba6fdcca8e567e2fc/O-Grande-Incendio-Florestal-de-Pedrogao-Grande.pdf 2017.

Di Virgilio, G., Evans, J. P., Blake, S. A., Armstrong, M., Dowdy, A. J., Sharples, J., and McRae, R.: Climate change increases the potential for extreme wildfires, Geophys. Res. Lett., 46, 8517–8526, 2019.

Duane, A., Castellnou, M., and Brotons, L.: Towards a comprehensive look at global drivers of novel extreme wildfire events, Climatic Change, 165, 1–21, 2021.

Forthofer, J., Shannon, K., and Butler, B.: Simulating diurnally driven slope winds with WindNinja. In In: Proceedings of 8th Eighth Symposium on Fire and Forest Meteorology, October 13–15 2009, Kalispell, MT, Boston, MA: American Meteorological Society, 13 pp., https://ams.confex.com/ams/8Fire/techprogram/paper_156275.htm (last access: 11 February 2022), 2009.

Friedlingstein, P., Jones, M. W., O'Sullivan, M., Andrew, R. M., Hauck, J., Peters, G. P., Peters, W., Pongratz, J., Sitch, S., Le Quéré, C., Bakker, D. C. E., Canadell, J. G., Ciais, P., Jackson, R. B., Anthoni, P., Barbero, L., Bastos, A., Bastrikov, V., Becker, M., Bopp, L., Buitenhuis, E., Chandra, N., Chevallier, F., Chini, L. P., Currie, K. I., Feely, R. A., Gehlen, M., Gilfillan, D., Gkritzalis, T., Goll, D. S., Gruber, N., Gutekunst, S., Harris, I., Haverd, V., Houghton, R. A., Hurtt, G., Ilyina, T., Jain, A. K., Joetzjer, E., Kaplan, J. O., Kato, E., Klein Goldewijk, K., Korsbakken, J. I., Landschützer, P., Lauvset, S. K., Lefèvre, N., Lenton, A., Lienert, S., Lombardozzi, D., Marland, G., McGuire, P. C., Melton, J. R., Metzl, N., Munro, D. R., Nabel, J. E. M. S., Nakaoka, S.-I., Neill, C., Omar, A. M., Ono, T., Peregon, A., Pierrot, D., Poulter, B., Rehder, G., Resplandy, L., Robertson, E., Rödenbeck, C., Séférian, R., Schwinger, J., Smith, N., Tans, P. P., Tian, H., Tilbrook, B., Tubiello, F. N., van der Werf, G. R., Wiltshire, A. J., and Zaehle, S.: Global Carbon Budget 2019, Earth Syst. Sci. Data, 11, 1783–1838, https://doi.org/10.5194/essd-11-1783-2019, 2019.

Giglio, L., Justice, C., Boschetti, L., and Roy, D.: MCD64A1 MODIS/Terra+ Aqua Burned Area Monthly L3 Global 500 m SIN Grid V006, NASA EOSDIS Land Processes DAAC: Sioux Falls, SD, USA, [data set], https://doi.org/10.5067/MODIS/MCD64A1.006, 2015.

Haines, D. A. and Service, U. F.: A lower atmospheric severity index for wildland fires, available at: https://www.frames.gov/catalog/11664 (last access: 14 February 2022), 1988.

Hersbach, H.: The ERA5 Atmospheric Reanalysis, in: AGU fall meeting abstracts, https://ui.adsabs.harvard.edu/abs/2016AGUFMNG33D..01H/abstract (last access: 10 February 2021), 2016.

Keetch, J. J. and Byram, G. M.: A drought index for forest fire control, vol. 38, US Department of Agriculture, Forest Service, Southeastern Forest Experiment, available at: https://www.fs.usda.gov/treesearch/pubs/40 (last access: 11 February 2022), 1968.

Khaykin, S., Legras, B., Bucci, S., Sellitto, P., Isaksen, L., Tence, F., Bekki, S., Bourassa, A., Rieger, L., Zawada, D., Jumelet, J., and Godin-Beekmann, S.: The 2019/20 Australian wildfires generated a persistent smoke-charged vortex rising up to 35 km altitude, Communications Earth & Environment, 1, 1–12, https://doi.org/10.1038/s43247-020-00022-5, 2020.

KingaD, A.: A method for stochastic optimization, Anon. InternationalConferenceon Learning Representations, SanDego, arXiv [preprint], arXiv:1412.6980 2015.

Kraskov, A., Stögbauer, H., and Grassberger, P.: Estimating mutual information, Phys. Rev. E, 69, 066138, https://doi.org/10.1103/PhysRevE.69.066138, 2004.

Lareau, N., Nauslar, N., and Abatzoglou, J. T.: The Carr Fire vortex: a case of pyrotornadogenesis?, Geophys. Res. Lett., 45, 13–107, 2018a.

Lareau, N. P. and Clements, C. B.: Environmental controls on pyrocumulus and pyrocumulonimbus initiation and development, Atmos. Chem. Phys., 16, 4005–4022, https://doi.org/10.5194/acp-16-4005-2016, 2016.

Lareau, N. P., Nauslar, N. J., and Abatzoglou, J. T.: The Carr Fire Vortex: A Case of Pyrotornadogenesis?, Geophys. Res. Lett., 45, 13107–13115, https://doi.org/10.1029/2018GL080667, 2018b.

Leach, R. N. and Gibson, C. V.: Assessing the Potential for Pyroconvection and Wildfire Blow Ups, Journal of Operational Meteorology, 9, 47–61, https://doi.org/10.15191/nwajom.2021.0904, 2021.

Lombardo, K. A. and Colle, B. A.: Convective storm structures and ambient conditions associated with severe weather over the northeast United States, Weather Forecast., 26, 940–956, 2011.

Mandel, J., Beezley, J. D., and Kochanski, A. K.: Coupled atmosphere-wildland fire modeling with WRF-fire, arXiv [preprint], arXiv:1102.1343, 2011.

McArthur, A.: Fire behaviour in eucalyptus forests, vol. 107, Commonw. Aust., Dep. Nat. Devel., Forest and Timber Bureau, Canberra, Leaflet n107, 36 pp., 1967.

McRae, R. H. D., Sharples, J. J., and Fromm, M.: Linking local wildfire dynamics to pyroCb development, Nat. Hazards Earth Syst. Sci., 15, 417–428, https://doi.org/10.5194/nhess-15-417-2015, 2015.

Mell, W., Jenkins, M. A., Gould, J., and Cheney, P.: A physics-based approach to modelling grassland fires, Int. J. Wildland Fire, 16, 1–22, 2007.

Moncrieff, M. W. and Miller, M. J.: The dynamics and simulation of tropical cumulonimbus and squall lines, Q. J. Roy. Meteor. Soc., 102, 373–394, 1976.

Morvan, D. and Frangieh, N.: Wildland fires behaviour: wind effect versus Byram's convective number and consequences upon the regime of propagation, Int. J. Wildland Fire, 27, 636–641, 2018.

Pausas, J. G. and Keeley, J. E.: A burning story: the role of fire in the history of life, BioScience, 59, 593–601, 2009.

Pausas, J. G. and Keeley, J. E.: Epicormic resprouting in fire-prone ecosystems, Trends Plant Sci., 22, 1008–1015, 2017.

Pedregosa, F., Varoquaux, G., Gramfort, A., Michel, V., Thirion, B., Grisel, O., Blondel, M., Prettenhofer, P., Weiss, R., Dubourg, V., Vanderplas, J., Passos, A., Cournapeau, D., Brucher, M., Perrot, M., and Duchesnay, E.: Scikit-learn: Machine Learning in Python, J. Mach. Learn. Res., 12, 2825–2830, 2011.

Pinto, M. M., DaCamara, C. C., Hurduc, A., Trigo, R. M., and Trigo, I. F.: Enhancing the fire weather index with atmospheric instability information, Environ. Res. Lett., 15, 0940b7, https://doi.org/10.1088/1748-9326/ab9e22, 2020.

Pirsko, A. R., Sergius, L. M., and Hickerson, C. W.: Causes and behavior of a tornadic fire-whirlwind, Res. Note PSW-RN-061, Berkeley, CA, US Department of Agriculture, Forest Service, Pacific Southwest Forest and Range Experiment Station,

61, 13 pp., available at: https://www.fs.usda.gov/treesearch/pubs/42171 (last access: 10 February 2022), 1965.

Potter, B.: The Haines Index – it's time to revise it or replace it, Int. J. Wildland Fire, 27, 437–440, 2018a.

Potter, B. E.: The role of released moisture in the atmospheric dynamics associated with wildland fires, Int. J. Wildland Fire, 14, 77–84, 2005.

Potter, B. E.: Quantitative Evaluation of the Haines Index's Ability to Predict Fire Growth Events, Atmosphere, 9, 177, https://doi.org/10.3390/atmos9050177, 2018b.

Ross, B. C.: Mutual information between discrete and continuous data sets, PloS One, 9, 1–5, https://doi.org/10.1371/journal.pone.0087357, 2014.

Rothermel, R. C.: A mathematical model for predicting fire spread in wildland fuels, Res. Pap. INT-115, Ogden, UT: U.S. Department of Agriculture, Intermountain Forest and Range Experiment Station, 40 pp., available at: https://www.fs.usda.gov/treesearch/pubs/32533 (last access: 10 February 2022), 1972.

San-Miguel-Ayanz, J., Schulte, E., Schmuck, G., Camia, A., Strobl, P., Liberta, G., Giovando, C., Boca, R., Sedano, F., Kempeneers, P., McInerney, D., Withmore, C., Santos de Oliveira, S., Rodrigues, M., Durrant, T., Corti, P., Oehler, F., Vilar, L., and Amatulli, G.: Comprehensive monitoring of wildfires in Europe: the European forest fire information system (EFFIS), in: Approaches to managing disaster-Assessing hazards, emergencies and disaster impacts, IntechOpen, https://doi.org/10.5772/28441, 2012.

San-Miguel-Ayanz, J., Oom, D., Artes, T., Viegas, D., Fernandes, P., Faivre, N., Freire, S., Moore, P., Rego, F., and Castellnou, M.: Forest fires in Portugal in 2017, in: Science for Disaster Risk Management 2020: acting today, protecting tomorrow, edited by: Casajus Valles, A., Marin Ferrer, M., Poljansek, K., and Clark, I., Publications Office of the European Union, Luxembourg, https://doi.org/10.2760/438998, 2019.

Shi, Y., Matsunaga, T., Saito, M., Yamaguchi, Y., and Chen, X.: Comparison of global inventories of CO_2 emissions from biomass burning during 2002–2011 derived from multiple satellite products, Environ. Pollut., 206, 479–487, 2015.

Short, K. C.: Spatial wildfire occurrence data for the United States, 1992–2015, Forest Service Research Data Archive [data set], https://doi.org/10.2737/RDS-2013-0009.4, 2017.

Sullivan, A. L.: Inside the inferno: fundamental processes of wildland fire behaviour, Current Forestry Reports, 3, 150–171, 2017.

Tory, K. and Kepert, J.: Pyrocumulonimbus Firepower Threshold: Assessing the atmospheric potential for pyroCb, Weather Forecast., 36, 439–456, 2021.

Tory, K. J., Thurston, W., and Kepert, J. D.: Thermodynamics of pyrocumulus: A conceptual study, Mon. Weather Rev., 146, 2579–2598, 2018.

Van Wagner, C. E.: Structure of the Canadian forest fire weather index, vol. 1333, Environment Canada, Forestry Service, https://cfs.nrcan.gc.ca/publications?id=19927 (last access: 10 February 2022), 1974.

Vitolo, C., Di Giuseppe, F., Barnard, C., Coughlan, R., San-Miguel-Ayanz, J., Libertà, G., and Krzeminski, B.: ERA5-based global meteorological wildfire danger maps, Scientific Data, 7, 1–11, 2020.

Williams, E. and Renno, N.: An analysis of the conditional instability of the tropical atmosphere, Mon. Weather Rev., 121, 21–36, 1993.